Available online at www.sciencedirect.com
ScienceDirect
Applied Mathematical Modelling 32 (2008) 1255–1280
APPLIED MATHEMATICAL MODELLING
www.elsevier.com/locate/apm

Modelling the impact of wind stress and river discharge on Danshuei River plume

Wen-Cheng Liu [a,*], Wei-Bo Chen [b], Ralph T. Cheng [c], Ming-Hsi Hsu [d]

[a] *Department of Civil and Disaster Prevention Engineering, National United University, Miao-Li 36003, Taiwan*
[b] *National Center for Ocean Research, National Taiwan University, Taipei 10617, Taiwan*
[c] *US Geological Survey, Menlo Park, CA 94025, USA*
[d] *Department of Bioenvironmental Systems Engineering, National Taiwan University, Taipei 10617, Taiwan*

Received 1 July 2006; received in revised form 1 March 2007; accepted 26 March 2007
Available online 22 April 2007

Abstract

A three-dimensional, time-dependent, baroclinic, hydrodynamic and salinity model, UnTRIM, was performed and applied to the Danshuei River estuarine system and adjacent coastal sea in northern Taiwan. The model forcing functions consist of tidal elevations along the open boundaries and freshwater inflows from the main stream and major tributaries in the Danshuei River estuarine system. The bottom friction coefficient was adjusted to achieve model calibration and verification in model simulations of barotropic and baroclinic flows. The turbulent diffusivities were ascertained through comparison of simulated salinity time series with observations. The model simulation results are in qualitative agreement with the available field data.

The validated model was then used to investigate the influence of wind stress and freshwater discharge on Dasnhuei River plume. As the absence of wind stress, the anticyclonic circulation is prevailed along the north to west coast. The model results reveal when winds are downwelling-favorable, the surface low-salinity waters are flushed out and move to southwest coast. Conversely, large amounts of low-salinity water flushed out the Danshuei River mouth during upwelling-favorable winds, as the buoyancy-driven circulation is reversed. Wind stress and freshwater discharge are shown to control the plume structure.

Keywords: River plume; Three-dimensional model; Danshuei River estuarine system and coastal sea; Freshwater discharge; Wind stress; Taiwan

1. Introduction

The costal ocean is the recipient of freshwater and land drained materials that are primarily brought in through river discharge. From the dynamical viewpoint the discharge site (the ''river mouth'') can be

* Corresponding author. Tel.: +886 37 381674; fax: +886 37 326567.
E-mail address: wcliu@nuu.edu.tw (W.-C. Liu).

0307-904X/$ - see front matter © 2007 Elsevier Inc. All rights reserved.
doi:10.1016/j.apm.2007.03.009

considered the source both momentum and buoyancy, produced by the release of light fluid into a heavier (more dense) ambient. The resulting dynamical structure is referred to as a (buoyant) river plume [1].

River waters have been regards as means for drinking water supply, maintenance of wild life and transportation, while their natural content in perceptible amounts of nutrients has always influenced the ecology of the receiving waters, which directly affects the food supply. In modern times, population growths of coastal states and technology-related development have added a plethora of man-made waste products on the river intake. These "materials" are carried by rivers (in solution, in suspension or as bed load) to their discharge site. It is becoming increasingly necessary to be able to control the impact of this type of 'imported" pollution in the coastal areas, which continue to be favored as rapidly growing population and recreation sites. Furthermore, the freshening of nearshore waters due to river runoff is one of the mechanisms that control circulation in coastal areas [2]. The present study is motivated by the need to understand and predict the phenomena that control the fate of riverine waters and related materials, taking into account the complex geomorphology that characterizes the Danshuei River system and its coastal sea.

Numerical studies of river plume have mostly concentrated on idealized model domains, so that results could be validated analytically and nondimensional numbers characteristic of plume dynamics could be derived. Such studies concentrate on plume dynamics [1,3–7]. These studies pointed out that, when the buoyant discharge is the only forcing mechanism, a "typical" mid-latitude plume develops after (a) the initial rigorous mixing caused by turbulence and friction and (b) the subsequent balance between Coriolis and the density-induced pressure gradient. The structure of a river plume includes an offshore bulge that extends anticyclonically seaward from the river mouth and the coastal current region that develops along a narrow nearshore strip to the right of the river mouth. Wind stress may either enhance or oppose the density-driven coastal current. Kourafalou et al. [1] showed that downwelling favorable winds strengthen the coastal current plume region and confine the bulge nearshore, while upwelling favorable winds may reverse the coastal current and allow a wide offshore bulge. Kourafalou et al. [8] studied, under realistic conditions, the wind and tidal influences on a river plume along the Southeast US continental shelf during spring season. Mikhailova and Shapiro [9] included the interaction between riverine low-salinity waters and abyssal upwelled waters in the Black Sea. Garvine [10] investigated the dependence of the alongshelf penetration of an unforced buoyant coastal discharge in parameters such as bottom slope, background diffusivity, tidal amplitude, and river discharge. Berdeal et al. [11] used a three-dimensional model (ECOM3d) to simulate the response of a high discharge river plume to an alongshore ambient flow and wind forcing. Arnoux-Chiavassa [12] used a higher order advection scheme to simulate 3D Rhone river plume. Lacroix et al. [13] described the distribution and variability of the salinity in Belgian coastal waters and determined the relative impact of the Scheldt and Rhine/Meuse freshwater plume. Whitney and Garvine [14] simulated the Delaware Bay buoyant outflow and compared results with observations of estuarine and shelf conditions.

The numerical simulation in realistic cases contributed to the understanding of the dynamics and the structure of the plumes by taking into account real bathymetries. A number of numerical models have applied to investigate the river plume in different continental shelves and estuaries overall the world. However there is not any report regarding to the Danshuei River plume in Taiwan. A number of three-dimensional hydrodynamic models are available to simulate the tidal current, salinity, and temperature in estuaries and coastal seas [15–21]. In the present study, a three-dimensional hydrodynamic model, UnTRIM [18,22], was implemented and applied to examine the impact of wind stress and freshwater discharge on river plume development in the Danshuei River coastal sea of northern Taiwan. Before the performance of model application, model validation was conducted with water surface elevation, current, and salinity and compared them with available field data in the Danshuei River estuarine system. Because of the unstructured gird applied in the model, the grids generation is easily to produce and to fit the topography. Moreover, the UnTRIM model takes the advantage to develop the water quality and sediment models in the future work.

2. Study site

The Danshuei River estuary (Fig. 1a) is the largest estuarine system in Taiwan, with its drainage basin including the capital city of Taipei. The tidal influence spans a total length of about 82 km, encompassing the entire length of the Danshuei River and the downstream reaches of its three major tributaries: the Tahan

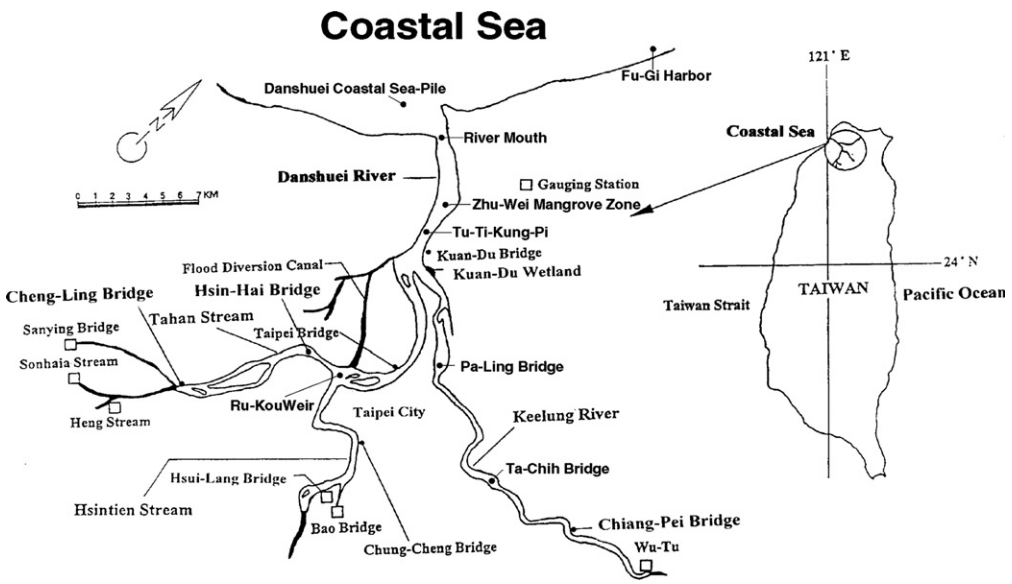

Fig. 1a. The map of the Danshuei River estuarine system and its adjacent coastal sea.

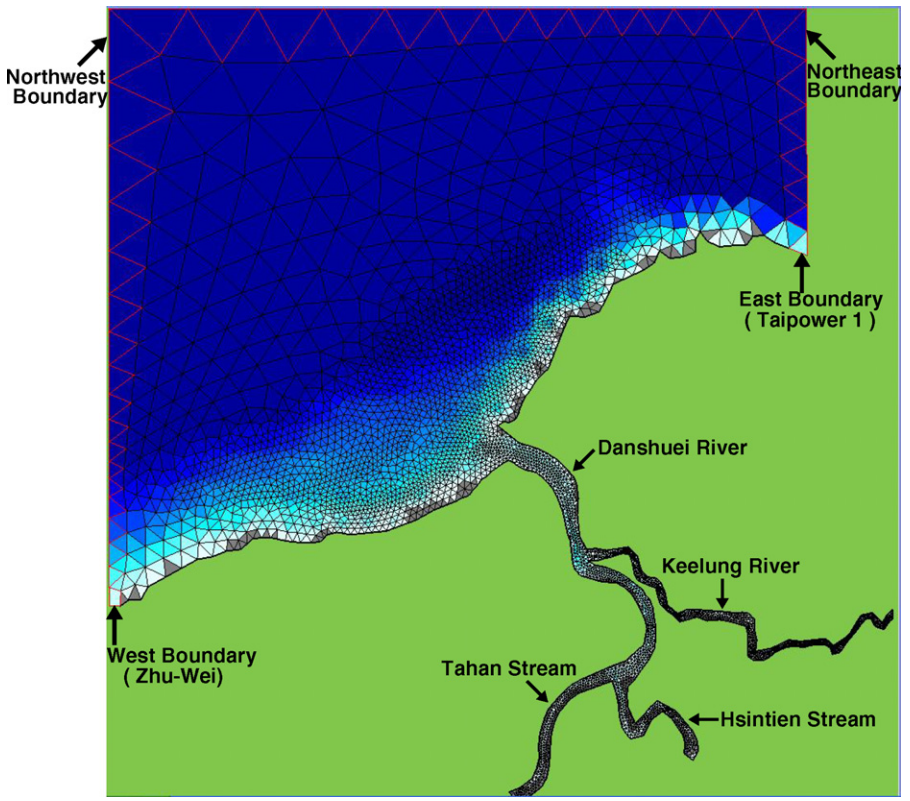

Fig. 1b. An unstructured model grid representing the modelling domain.

Stream, the Hsintien Stream, and the Keelung River. The average river discharges at the upstream limits of tide are 41.7 m^3/s, 72.4 m^3/s, and 25.5 m^3/s, respectively, in the Tahan Stream, Hsintien Stream, and Keelung River. The northeast wind prevails during the autumn and winter seasons, while the southwest wind prevails

during the spring and summer seasons in Taiwan. The moderate to strong wind speed ranges from 6 to 15 m/s [23]. Except during a flooding event, the astronomical tide may reach as far upriver as Cheng-Ling Bridge in Tahan Stream, the Hsiu-Lang Bridge in Hsintien Stream and the Chiang-Pei Bridge in Keelung River (Fig. 1a). Tidal propagation into the estuary from coastal ocean is the dominant mechanism controlling the variations of water surface elevation, and ebb and flood flows. The M_2 tide is the primary tidal constituent at the river mouth, with a mean tidal range of 2.17 m, and up to 3 m at spring tides. Because of the cross-sectional contraction and wave reflection, the mean tidal range may reach a maximum of 2.39 m within the system. The phase relationship between tidal elevation and tidal flow is close to standing wave characteristics [24].

Sea water intrudes upriver as a result of tidal dispersion and residual circulation. Salinity varies in intratidal time scale in response to the ebb and flood of tidal flows as well as in response to changing freshwater inflows. The limit of salt intrusion may reach beyond 25 km in the Tahan Stream from river mouth during the period of low flow. The baroclinic pressure gradient due to longitudinal salinity/density distribution is large enough to push the denser salt water upriver along the bottom layer of the estuary forming the classical two-layer estuarine circulation [25–27].

In this study, a baroclinic 3 D model, UnTRIM, is used to cover the Danshuei River estuarine system and adjacent coastal sea where the bathymetry is gradually getting deeper away from the coastline (Fig. 1a), and the model uses an unstructured model grid as shown in Fig. 1b. Wang [28] used a towed-ADCP to measure the tidal current at the coastal sea off the Danshuei River. The maximum tidal current near the river mouth can reach 1.25 m/s and the tidal current fluctuates with flood and ebb tides along the coastline. The measured mean flow at the upper 10 m is about 0.5 m/s. The flow decreases with increasing depth; the mean current is about 0.35 m/s at 10–40 m and 0.2 m/s below 40 m of depth.

3. Model description

3.1. Governing equation

The governing equations describing three-dimensional free-surface flows are the well known shallow water equations. Such equations express the physical conservation principles of volume, mass, and momentum.

The volume conservation is expressed by the following incompressibility condition:

$$\frac{\partial u}{\partial x}+\frac{\partial v}{\partial y}+\frac{\partial w}{\partial z}=0, \tag{1}$$

where $u(x, y, z, t)$, $v(x, y, z, t)$, and $w(x, y, z, t)$ are the velocity components in the horizontal x, y, and vertical z-directions, respectively,

Integrating the continuity equation (1) over depth and using a kinematic condition at the free-surface leads to the following free-surface equation [16]:

$$\frac{\partial \eta}{\partial t}+\frac{\partial}{\partial x}\left[\int_{-h}^{\eta} u\mathrm{d}z\right]+\frac{\partial}{\partial y}\left[\int_{-h}^{\eta} v\mathrm{d}z\right]=0, \tag{2}$$

where t is the time; $h(x, y)$ is the prescribed bathymetry measured from the undisturbed water surface and $\eta(x, y, t)$ is the free-surface elevation. Thus, $H(x, y, t)=h(x, y)+\eta(x, y, t)$ is the total water depth.

The mass conservation of salt (solutes) is expressed by the following differential equation:

$$\frac{\partial S}{\partial t}+u\frac{\partial S}{\partial x}+v\frac{\partial S}{\partial y}+w\frac{\partial S}{\partial z}=\frac{\partial}{\partial x}\left(K^{\mathrm{h}}\frac{\partial S}{\partial x}\right)+\frac{\partial}{\partial y}\left(K^{\mathrm{h}}\frac{\partial S}{\partial y}\right)+\frac{\partial}{\partial z}\left(K^{\mathrm{v}}\frac{\partial S}{\partial z}\right), \tag{3}$$

where S is the salinity; K^{h} and K^{v} are prescribed non-negative horizontal and vertical diffusivities, respectively.

Under the hydrostatic approximation, the vertical accelerations in the vertical momentum equation can be neglected.

The hydrostatic pressure $p(x, y, z, t)$ can be expressed as

$$p(x,y,z,t)=p_{\mathrm{a}}(x,y,t)+g[\eta(x,y,t)-z]+g\int_{z}^{\eta}\frac{\rho-\rho_0}{\rho_0}\mathrm{d}\zeta, \tag{4}$$

where p_a is the atmospheric pressure; g is the gravitational acceleration; ρ is the water density; ρ_o is the freshwater density.

The horizontal momentum equations can also be written as

$$\frac{Du}{Dt} - fv = -\frac{\partial p_a}{\partial x} - g\frac{\partial \eta}{\partial x} - g\frac{\partial}{\partial x}\left[\int_z^\eta \frac{\rho-\rho_0}{\rho}d\varsigma\right] + v^h\left(\frac{\partial^2 u}{\partial x^2}+\frac{\partial^2 u}{\partial y^2}\right) + \frac{\partial}{\partial z}\left(v^v\frac{\partial u}{\partial z}\right), \tag{5}$$

$$\frac{Dv}{Dt} + fu = -\frac{\partial p_a}{\partial y} - g\frac{\partial \eta}{\partial y} - g\frac{\partial}{\partial y}\left[\int_z^\eta \frac{\rho-\rho_0}{\rho}d\varsigma\right] + v^h\left(\frac{\partial^2 v}{\partial x^2}+\frac{\partial^2 v}{\partial y^2}\right) + \frac{\partial}{\partial z}\left(v^v\frac{\partial v}{\partial z}\right), \tag{6}$$

where $D(\ )/Dt$ is the substantive derivative; f is the Coriolis parameter; v^h and v^v are, respectively, the coefficients of horizontal and vertical eddy viscosity.

The vertical momentum is expressed as

$$\frac{Dw}{Dt} = v^h\left(\frac{\partial^2 w}{\partial x^2}+\frac{\partial^2 w}{\partial y^2}\right) + \frac{\partial}{\partial z}\left(v^v\frac{\partial w}{\partial z}\right). \tag{7}$$

The system is closed by an equation of state which relates the water density to the concentration of salinity (contributions from temperature variations to density are neglected). The equation of state takes the form of

$$\rho = \rho_0(1+kS), \tag{8}$$

where k is constant ($=7.8\times10^{-4}\ \mathrm{ppt}^{-1}$).

3.2. Turbulence closure model

In most estuaries with a significant freshwater discharge, salinity may serve as an idea natural tracer for calibration of mixing processes. Salinity distribution in an estuary is affected by the tidal current, freshwater discharge, density circulation, as well as turbulent mixing processes. Therefore the salinity distribution reflects the combined results of all processes, and in turn it controls density circulation and modifies mixing processes [24].

In the present model, the mixing processes are modeled with turbulent diffusion terms. The mixing length concept is used to calculate eddy viscosity v^v and diffusion coefficient K^v in vertical direction.

The formations for v^v and K^v are

$$v^v = \alpha Z^2\left(1-\frac{Z}{h}\right)^2\left|\frac{\partial u}{\partial z}\right|(1+\beta R_i)^{-1/2}, \tag{9}$$

$$K^v = \alpha Z^2\left(1-\frac{Z}{h}\right)^2\left|\frac{\partial u}{\partial z}\right|(1+\beta R_i)^{-3/2}, \tag{10}$$

where Z is the distance from the surface, α is a constant to be determined empirically, and a local Richardson number (R_i) is used to characterize stability due to stratification, where the Richardson number is defined as

$$R_i = -\frac{g}{\rho}\left(\frac{\partial \rho}{\partial z}\right)\left(\frac{\partial u}{\partial z}\right)^{-2}. \tag{11}$$

The horizontal mixing coefficients (v^h and K^h) range from 1 to 100 m^2/s [29]. Since the horizontal length scales are several orders of magnitude larger than the vertical length scales, the horizontal mixing terms play a relatively insignificant role in momentum balance; they are retained in the model nevertheless. Constant values for v^h and K^h are used and they are adjusted, within the range of 1–100 m^2/s, through model calibration.

3.3. Numerical approximation

The numerical algorithm of UnTRIM is fundamentally the same as TRIM3D [16,30], except that the finite-difference treatment of the governing partial differential equations is performed over an unstructured grid mesh. Before discretizing the governing equations, the horizontal domain (x, y) is covered by a set of

non-overlapping convex polygons. Each side of a polygon is either a boundary line or a side an adjacent polygon. Moreover, it is assumed that within each polygon there exists a point (i.e., center) such that the segment joining the centers of two adjacent polygons and the side shared by the two polygons have a non-empty intersection and are orthogonal to each other (shown in Fig. 2). One such grid is called an unstructured orthogonal grid [17,31]. The center of a polygon does not necessarily coincide with its geometrical center. The special cases of unstructured orthogonal grids include the rectangular finite-difference grids, as well as a grid of uniform equilateral triangles. In these particular cases the center of each polygon can be identified with its geometrical center. Another example of an unstructured orthogonal grid is a set of Delaunay triangles where the triangulation includes only acute triangles [32].

A semi-implicit scheme define above is used in order to obtain an efficient numerical algorithm whose stability is independent from the free-surface gravity waves, wind stress, vertical viscosity and bottom friction. Consider a typical polygon, Fig. 2, the momentum equation, Eqs. (5) and (6), is finite-differenced in the normal direction of each vertical face along oa, ob, and oc directions. The momentum equation relates the gradient of water surface elevation between adjoining polygons and the face velocity on the common face between these polygons. As stated previously, the wind stress, the vertical mixing and the bottom friction are discretized implicitly for numerical stability.

An explicit finite-difference operator is used to account for the contributions from the discretization of the advection and horizontal dispersion terms. A particular form for this operator can be given in several ways, such as an Eulerian–Lagrangian scheme [16]. For stability, the implicitness factor θ has to be chosen in the range $\frac{1}{2} \leqslant \theta \leqslant 1$ [30]. Along the vertical direction, the model domain is discretized by fixed levels, not necessarily uniform, with which a simple finite-difference discretization is used. The vertical space increment is defined as the distance between two consecutive level surfaces. In general, the vertical thickness of the top and bottom layers can vary depending on the spatial location and the thickness of the top layer can also vary with time. The vertical space increment is allowed to vanish. In fact, this is how the wetting and drying of computational cells are accomplished.

For three-dimensional barotropic flow, the salt transport equation is un-coupled from the momentum equations. A non-negative bottom friction coefficient is specified by the Manning–Chezy formula [16]. If the advections are treated by an Eulerian–Lagrangian scheme with positive bottom friction, then the numerical scheme is unconditionally stable. For baroclinic flows, since the density gradient terms are expressed explicitly in the momentum equations, and the solutions of the transport variables are solved lagged one time-step. In this case, the numerical scheme is subject to a weak stability condition due to the explicit treatment of the density gradient terms in the momentum equations. For stability, the integration time step must be chosen so that the propagation of internal wave must satisfy the Courant–Friedrich–Lewy (CFL) condition. The necessary and sufficient stability condition is formed as [16]

$$\Delta t \leqslant \left[\frac{|u|}{\Delta x}+\frac{|v|}{\Delta y}+\frac{|w|}{\Delta z}+2v^{\mathrm{h}}\left(\frac{1}{\Delta x^2}+\frac{1}{\Delta y^2}\right)\right]^{-1}. \tag{12}$$

In addition, the numerical scheme is also subject to a weak stability condition due to the explicit treatment of the horizontal diffusion in the momentum equations.

3.4. Grid generation

Many factors affect flows in the estuarine system and its adjacent coastal sea, but the bathymetry is the most important factor. An accurate bathymetric representation by the model grid is the most important and fundamental requirement in a successful modelling study [33,34]. This is particularly true for the Danshuei River estuarine system and adjacent coastal sea, where the bathymetric variations are very complex. The model grid must represent accurately the characteristics of the Danshuei River estuarine system that constitutes the model domain.

The UnTRIM model uses an unstructured grid, some aspects of the grid definition file are similar to those used in finite-element applications, therefore the literatures on grid generation for finite-elements apply in

UnTRIM applications. For the purpose of generating an unstructured model grid for UnTRIM model application, a commercial software for mesh generation, Argus software [35], has been adopted.

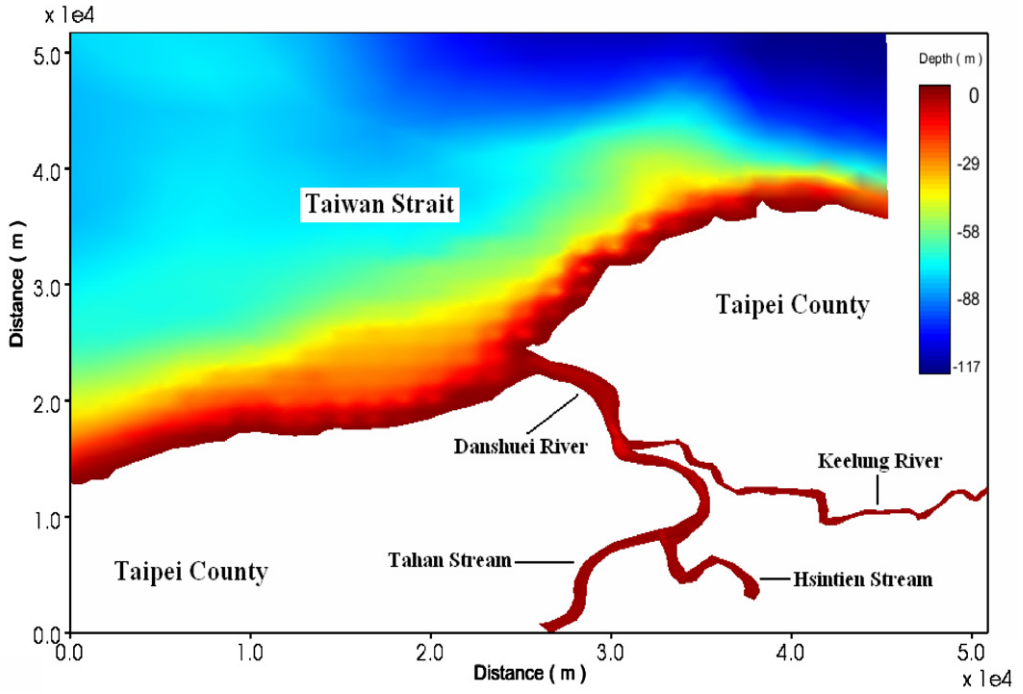

Fig. 1c. The contour of Danshuei River estuarine system and adjacent coastal sea.

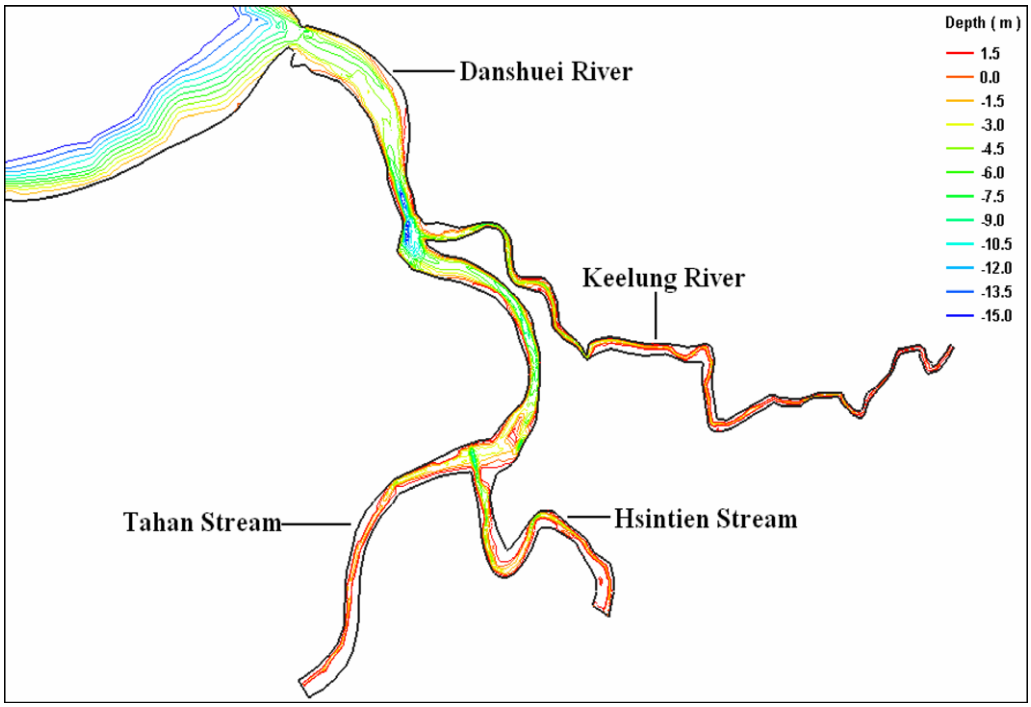

Fig. 1d. The contour focusing on the Danshuei River estuarine system.

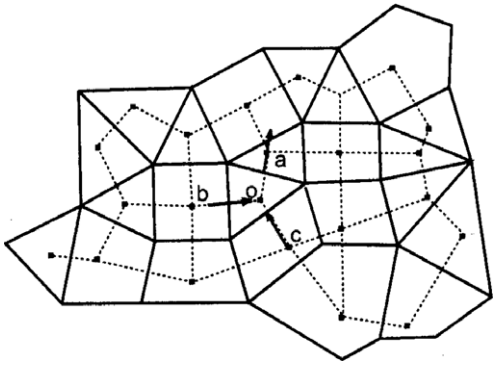

Fig. 2. Orthogonal unstructured grid (oa, ob, and oc present the intersection in the normal direction of each vertical face).

The original bathymetry data used in this study were obtained from National Center for Ocean Research and Water Resources Agency, Taiwan. The deepest depth within the study area is 110 m (below the mean sea level) near the northeast corner of the model in the coastal sea. The model mesh for the Danshuei River estuarine system and its adjacent coastal sea consists of 8181 3- and 4-sided polygons (Fig. 1b). Higher resolution grids are used in the Danshuei River estuary, and coarser grids are used in the coastal sea. According to the bathymetry and topography in the Danshuei River estuarine system and adjacent coastal sea (Figs. 1c and 1d), sixty vertical layers are specified with the layer thickness varying from 1 m in the top 10 layers, 2 m for the other layers. For this model grid, 360 seconds time step was used in simulations without any sign of numerical stability.

4. Model validation

4.1. Calibration with amplitudes and phases

Hsu et al. [24] used a vertical two-dimensional hydrodynamic model to the Danshuei River estuarine system. They found that the bottom roughness is a significant parameter that affects the tidal amplitudes and phases along the Danshuei River estuarine system. To focus on a particular aspect of the dynamic forcing and simplify the calibration process, it is proposed that the model be tuned with astronomical tide only. The approach also eliminates the uncertainty caused by measured errors in the field data. The satisfactory comparison with field data will serve as verification that the model properly simulates all of the forcing combined.

Jan et al. [36] reported that five tidal-constituents (i.e., M_2, S_2, N_2, K_1, and O_1) are sufficient to represent the tidal dynamics in the Taiwan Strait. Therefore the five tidal-constituents according to Jan et al. [36] were adopted in the model simulation as a forcing function at the coastal sea boundaries. The amplitudes and phases used for the model simulation in the coastal sea are listed in Table 1. Amplitudes and phases of these five tidal constituents were used to generate time-series water surface elevation along the open boundaries for two-month model simulation. Harmonic analysis was performed on the time series of the model simulated

Table 1
The amplitudes and phases used for the model simulation at the coastal sea boundaries

Constituent	East boundary		Northeast boundary		West boundary		Northwest boundary	
	Amplitude (m)	Phase (°)	Amplitude (m)	Phase (°)	Amplitude (m)	Phase (°)	Amplitude (m)	Phase (°)
M_2	0.47	172.37	0.6711	171.33	0.1236	181.63	1.3716	180.42
S_2	0.12	331.75	0.1866	332.25	0.3452	354.5	0.3987	355.2
N_2	0.10	262.74	0.1370	262.35	0.2252	281.373	0.2526	279.41
K_1	0.21	232.33	0.2223	234.2	0.2121	246.06	0.2275	246.69
O_1	0.17	67.54	0.170	67.05	0.1748	75.02	0.1866	74.40

water surface elevation at various locations. Through the bottom friction coefficient represented by the Manning–Chezy formula in the model was adjusted carefully, the results are presented in Fig. 3. It shows

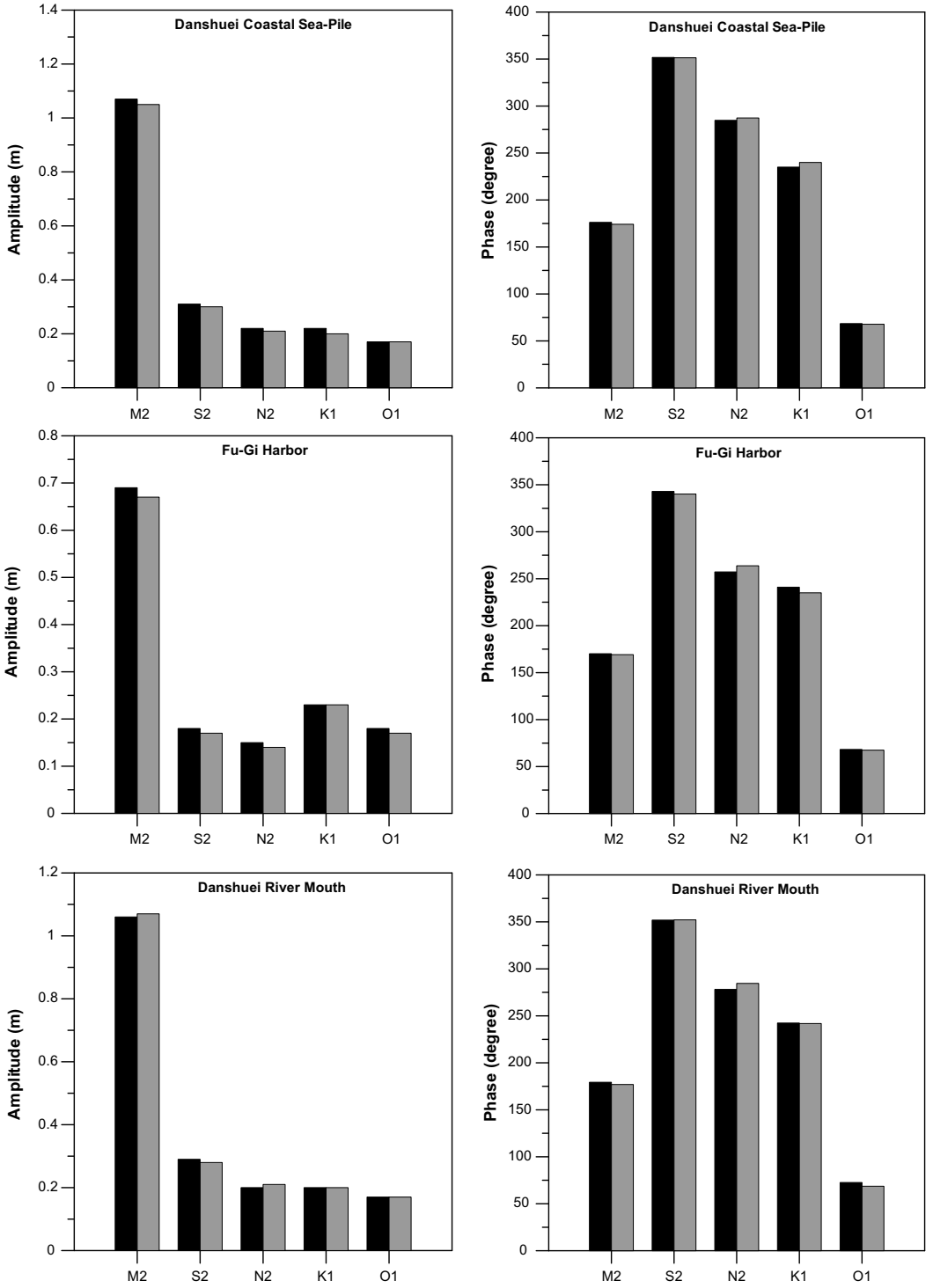

Fig. 3. Comparisons of amplitude and phase of five major tidal harmonics computed with the 3D model and obtained from tide measurements at nine stations: (■) observation, (▨) simulation.

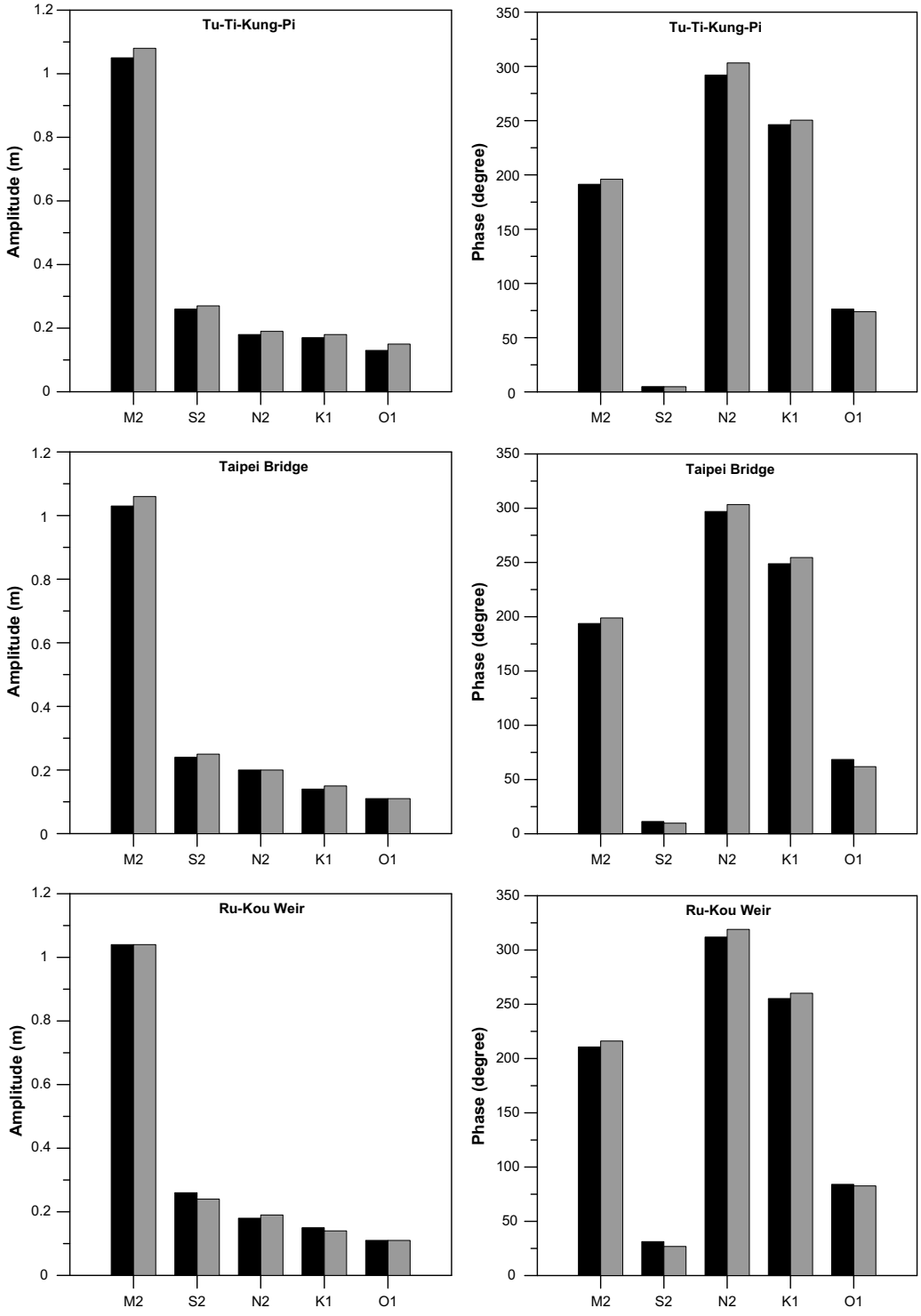

Fig. 3 (*continued*)

the comparison of the amplitudes and phases of harmonic constants between the computed and observed tides at nine locations. Table 2 presents that the calculated absolute mean difference and root-mean-square errors of

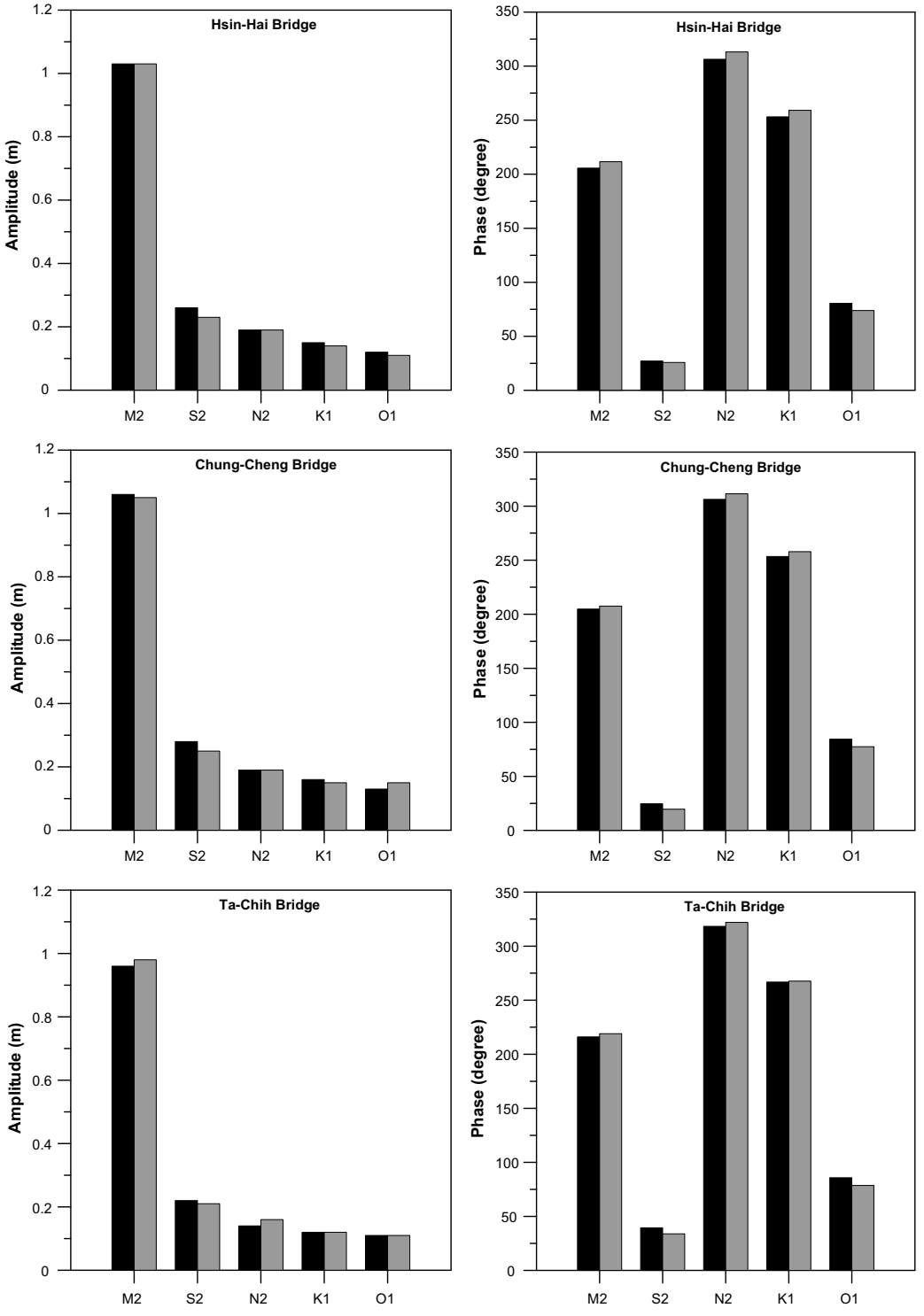

Fig. 3 (*continued*)

tidal constituents for amplitudes are in the ranges of 0.01–0.02 m and for phases are in the ranges of 2.4–6.7°. The differences in amplitudes and phases are quite small, and the water surface elevations are reasonably validated.

Table 2
The comparison of computed and observed amplitudes and phases of tidal constituents

Constituent	Danshuei Coastal Sea-Pile		Fu-Gi Harbor		Danshui River Mouth		Tu-Ti-Kung-Pi		Taipei Bridge	
	Observed	Simulated	Observed	Simulated	Observed	Simulated	Observed	Simulated	Observed	Simulated
(a) Amplitude (m)										
M_2	1.07	1.05	0.69	0.67	1.06	1.07	1.05	1.08	1.03	1.06
S_2	0.31	0.30	0.18	0.17	0.29	0.28	0.26	0.27	0.24	0.25
N_2	0.22	0.21	0.15	0.14	0.20	0.21	0.18	0.19	0.20	0.20
K_1	0.22	0.20	0.23	0.23	0.20	0.20	0.17	0.18	0.14	0.15
O_1	0.17	0.17	0.18	0.17	0.17	0.17	0.13	0.15	0.11	0.11
(b) Phase (°)										
M_2	176.18	174.19	170.18	169.17	179.34	176.96	191.38	196.08	193.80	198.93
S_2	351.8	351.42	342.96	340.16	351.90	352.21	4.88	4.76	11.29	9.81
N_2	284.74	287.34	257.24	263.74	278.21	284.53	292.02	303.23	296.98	303.38
K_1	235.00	239.93	241.00	234.97	242.30	241.87	246.35	250.50	248.86	254.58
O_1	68.47	67.78	68.25	67.44	72.60	68.67	76.35	73.93	68.47	61.82
	Ru-Kou Weir		Hsin-Hai Bridge		Chung-Cheng Bridge		Ta-Chih Bridge		AME	RMSE
	Observed	Simulated	Observed	Simulated	Observed	Simulated	Observed	Simulated		
(a) Amplitude (m)										
M_2	1.04	1.04	1.03	1.03	1.06	1.05	0.96	0.98	0.02	0.02
S_2	0.26	0.24	0.26	0.23	0.28	0.25	0.22	0.21	0.02	0.02
N_2	0.18	0.19	0.19	0.19	0.19	0.19	0.14	0.16	0.01	0.01
K_1	0.15	0.14	0.15	0.14	0.16	0.15	0.12	0.12	0.01	0.01
O_1	0.11	0.11	0.12	0.11	0.13	0.15	0.11	0.11	0.01	0.01
(b) Phase (°)										
M_2	210.68	216.10	205.64	211.55	204.82	207.55	216.05	219.00	3.58	3.94
S_2	31.32	26.85	27.10	25.81	24.65	19.60	39.43	33.82	2.39	3.14
N_2	311.91	319.02	306.34	313.16	306.26	311.42	318.38	321.99	6.27	6.69
K_1	255.28	260.19	253.11	259.14	253.44	257.90	266.81	267.66	4.17	4.62
O_1	84.08	82.65	80.50	73.83	84.38	77.47	85.83	78.65	4.08	4.86

AME: absolute mean error; RMSE: root-mean-square error.

4.2. Verification of water surface elevation, current, and salinity

The model verification was conducted with the daily freshwater discharges of the year 2000 as the forcing at the upstream boundaries. The open boundaries at the coastal sea were specified by five tidal-constituent (given in Table 1). The model was run for one-year simulation. The model results of time-series surface elevation, current and salinity were verified with field data in the same periods when field data are available. Because of the typhoon events and storm run-off, the peak freshwater discharges occurred on August 23 and 30. The freshwater discharge inputs from three tributaries (Tahan Stream, Hsintein Stream, and Keelung River) during the period of August 21–31, 2000 are shown in Fig. 4a, and during these eleven-days the computed surface elevations are compared with field data at several stations (Fig. 4c–i). The wind conditions were included in the model simulation (Fig. 4b). In general, the modelling results reproduce the water level variations very well. The water surface elevations at the upriver stations (Fig. 4g–i) have much more conspicuous response to pulses of high freshwater discharge, the modeled water levels follow the low water variations closely throughout the storm event. It demonstrates that the model can accurately reproduce water surface elevations even under extremely large variations of daily freshwater discharge input from three tributaries.

The Taiwan Water Resources Agency conducted 13 h (during daylight hours) intensified field measurement at five transects on May 5, 2000. Water velocities were measured half-hourly at several stations. Water speed was measured with handheld current meters by personnel on boats, the water directions were not measured.

As the velocity data were recorded by hand and "ebb or flood" directions were also noted based on visual observations. During slack tides, there were some difficulties (uncertainty) assigning current directions. Except

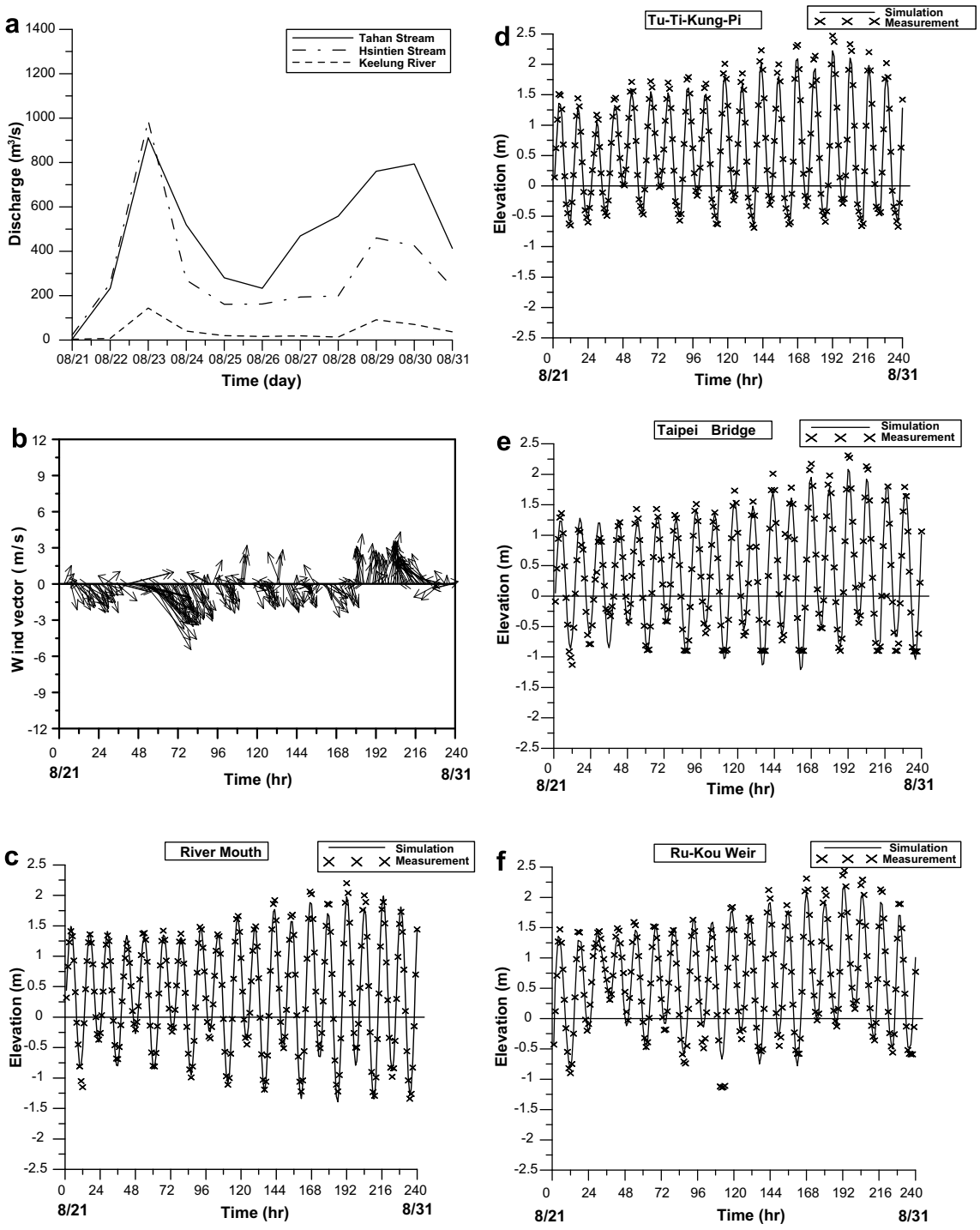

Fig. 4. (a) Freshwater discharge inputs from three tributaries during the period of August 21–31, 2000, (b) wind conditions, and the comparison of water surface elevation at: (c) Danshuei River mouth, (d) Tu-Ti-Kung-Pi, (e) Taipei Bridge, (f) Ru-Kou-Weir, (g) Hsin-Hai Bridge, (h) Chung-Cheng Bridge, and (i) Ta-Chih Bridge.

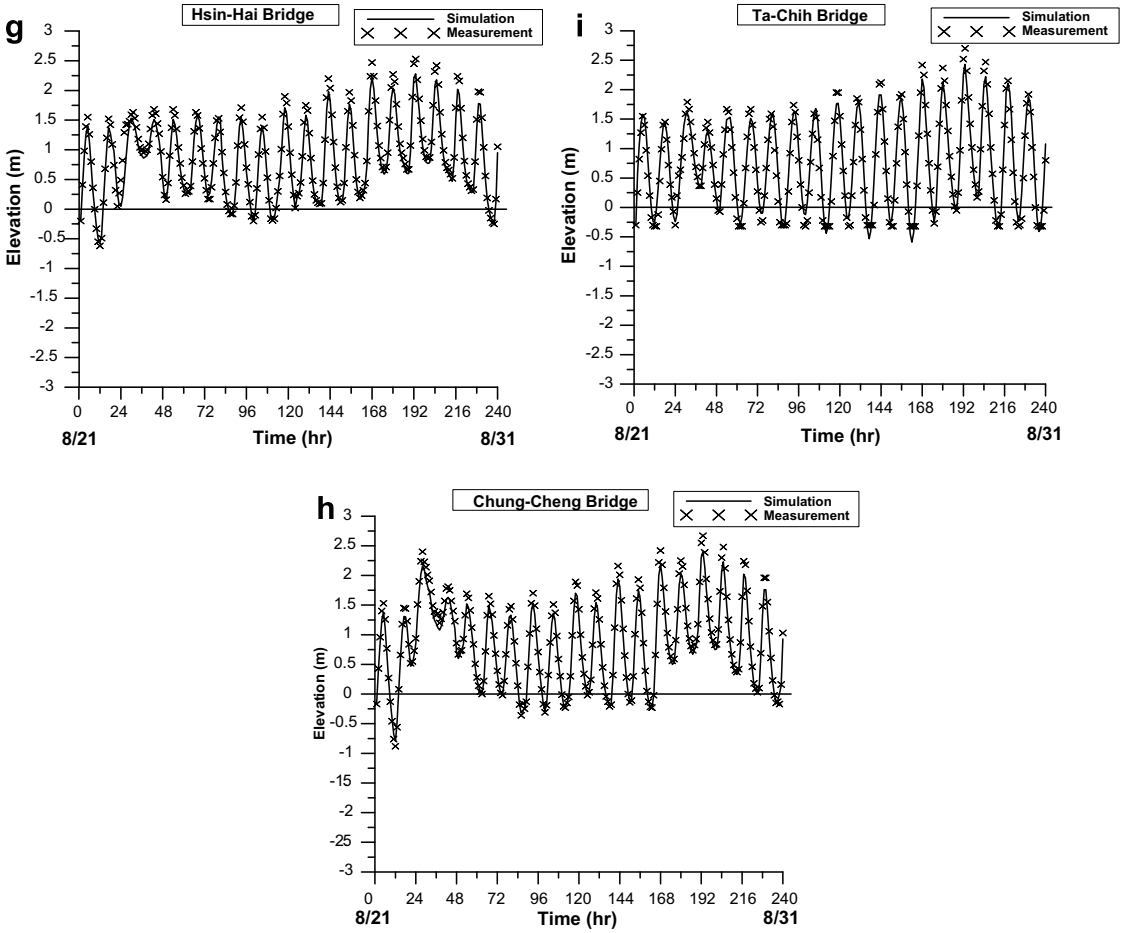

Fig. 4 (*continued*)

at those upriver transects close to tidal limits, the velocity measurements were made at two depths near bottom and near surface. The measured velocities near top and bottom are compared with model computed velocities at five stations: (a) Kuan-Du Bridge, (b) Taipei Bridge, (c) Hsin-Hai Bridge, (d) Chung-Cheng Bridge, and (e) Pa-Ling Bridge, Fig. 5a–e, for May 5, 2000. While there are a certain amount of uncertainties in these measurements (instrument limitations), these comparisons show that the model satisfactorily predicted the velocity in both the top and bottom layers along the channel.

In most estuaries when significant freshwater discharges and stratification exist, salinity becomes a natural conservative tracer for studying the mixing processes. Salinity distribution in an estuary is affected by the tidal current, freshwater discharge, as well as tidal and turbulent mixing processes. Therefore the resulting salinity distribution reflects the combined result of all processes, and in turn it controls (density) gravitational circulation and modifies mixing processes. Only limited long-term salinity time-series exists at the Zhu-Wei mangrove zone collected by the Taiwan Industrial Technology Institute; this time-series was used for model calibration and verification. In the numerical model, the salinities values at open boundaries at the coastal sea were set to 35 ppt. The salinity boundary conditions at heads of three tributaries were set to 0 ppt along with the specification of daily freshwater discharges. The wind conditions were included in the model simulation (Fig. 6b and e). Two one-week time periods were examined. During November 15 through November 22, 2000 (Fig. 6a), fresh-water discharge was receding from 300 m^3/s to about 150 m^3/s. The computed salinity time series compared very favorably with the discrete salinity measurements at the Zhu-Wei mangrove zone, Fig. 6c. The computed salinities reproduce the pattern of observed salinity variations in a dynamic variation of

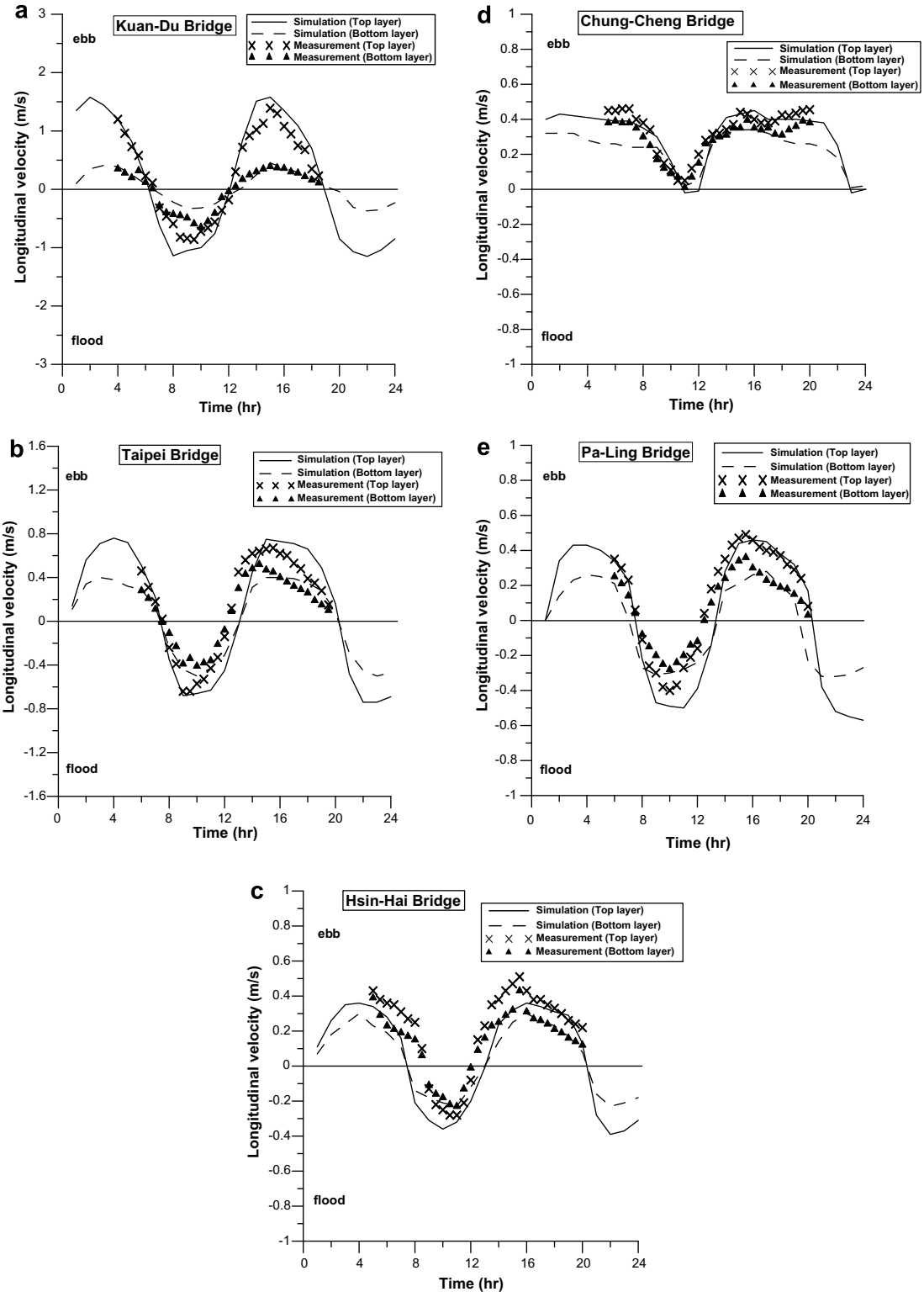

Fig. 5. The comparison of computed longitudinal velocity with time series data at: (a) Kuan-Du Bridge, (b) Taipei Bridge, (c) Hsin-Hai Bridge, (d) Chung-Cheng Bridge, and (e) Pa-Ling Bridge.

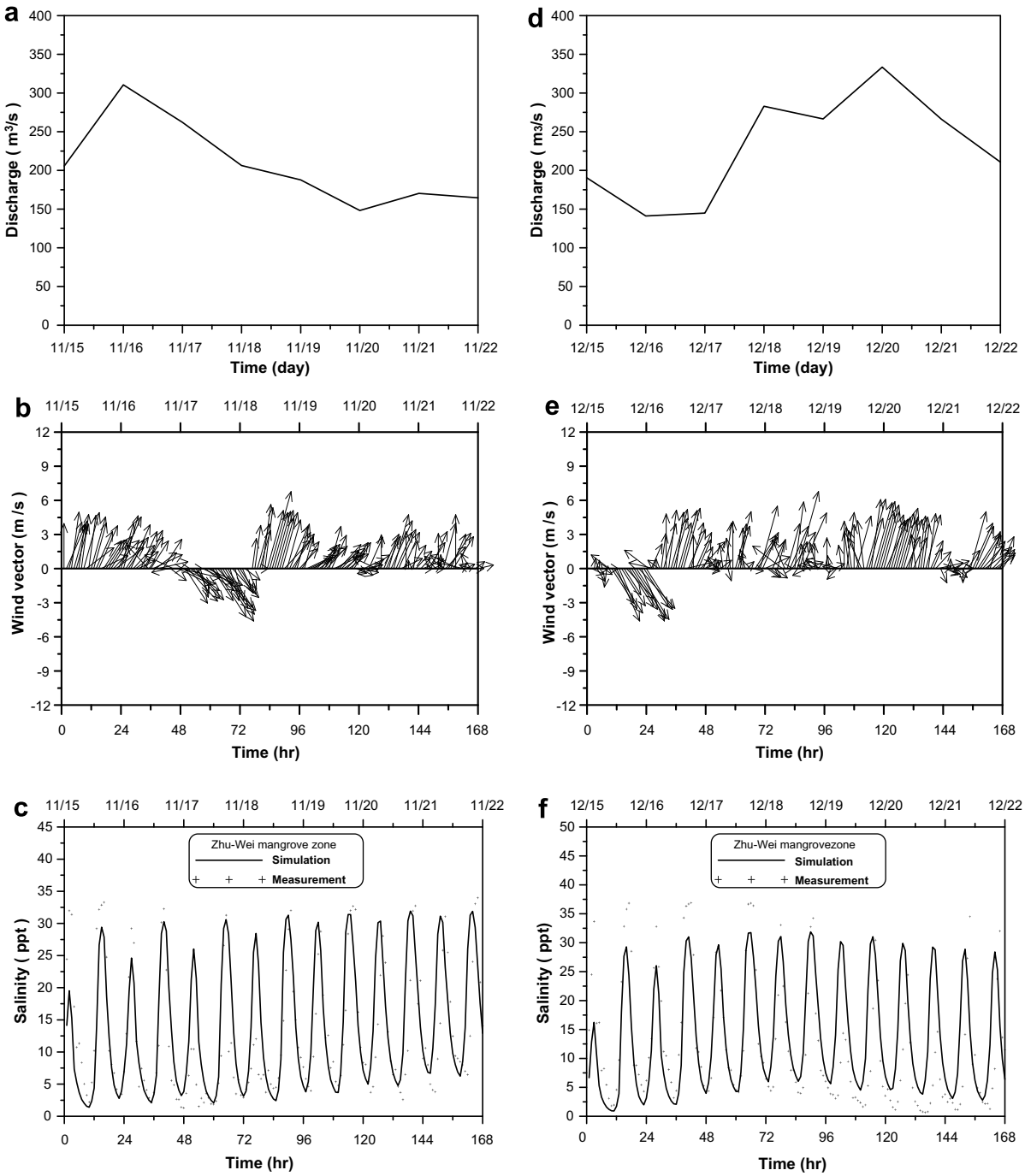

Fig. 6. The comparison of computed salinity with time series data at Zhu-Wei mangrove zone in 2000 (a) discharge, (b) wind, and (c) salinity from 15 to 22 November; (d) discharge, (e) wind, and (f) salinity from 15 to 22 December.

salinity between 0.0 and 33 ppt in a tidal cycle. The dynamic variations of salinity covered a range of about 30 ppt, and mean salinity value increased in response to decrease fresh water discharge. The salinity was measured at 1.5 m below surface and the computed salinity was taken from the surface layer, but salinity is generally well mixed in the vertical at this site. In the week between December 15 and 22, 2000, fresh water

discharge was in an increasing trend from 150 m^3/s to 300 m^3/s (Fig. 6d). While the measured salinity was as high as 37 ppt suggesting that substantial evaporation might be present but the evaporation mechanism was not built in the model. Nonetheless, the UnTRIM model reflected the large dynamic variations of salinity in a tidal cycle, and decreasing trend of mean salinity as fresh water increased near the end of this week. In these comparisons, the constants, $\alpha = 0.0115$ and $\beta = 0.75$, gave best results in the turbulence closure model.

5. Model investigations

5.1. Freshwater discharge forcing

River discharge constituents the most important forcing since there would be no estuary or buoyant outflow without freshwater input. The influence of river discharge on salinity intrusion and estuarine circulation has been investigated in the Danshuei River estuarine system [25,26], however the river plume characteristics have not really studied. The validated three-dimensional hydrodynamic model was then used to investigate the river plume in Danshuei River mouth to variations of freshwater discharge conditions. Five tidal constituents, M_2, S_2, N_2, K_1, and O_1, were used to generate a time series of water surface elevations as open boundary conditions and a constant salinity 35 ppt were specified at the coastal sea for a three-month model simulation. The amplitudes and phases used for model simulation at the coastal sea boundaries presented in Table 1. No wind stress forcing was considered in the model. The model was run with low flow (Q_{50}, a flow with an exceedence probability of 50%) and high flow (Q_{10}) conditions. The freshwater discharges at the upstream boundaries of the Tahan Stream, Hsintien Stream, and Keelung River were listed in Table 3.

Fig. 7 presents the tidally averaged salinity distribution under Q_{10} and Q_{50} flow conditions. A band of low-salinity water is formed along the coastline. When the freshwater discharge increases, the river plume distance is far from the coastline. The salinity (arbitrarily limited by the 34 isohaline) due to the river plume is located at the distance 3 km from the Danshuei River mouth under Q_{10} flow, while salinity is at 1–2 km distance from the Danshuei River mouth under Q_{50} flow condition. The high freshwater discharge results in the extension of low-salinity. The residual currents Q_{10} and Q_{50} flow conditions are shown in Fig. 8. The anticyclonic circulation is included along the north to west coast. The plumes and the buoyancy-driven coastal currents from the river are linked. The magnitude of the computed residual current is about 0.15–0.3 m/s that is the same order of magnitude measured by Wang [28]. With the pure freshwater discharge and tidal effects including in the model simulation, the results reveal that freshwater discharge exerts a significant impact on the plume distance and salinity distributions in Danshuei River coast region.

5.2. Wind stress forcing

In the experiments that follow, wind stress and tide are the forcing function, so the salinity remains constant and the velocity field is purely wind-driven. Five tidal constituents, M_2, S_2, N_2, K_1, and O_1, are forced at the sea boundaries (Table 1). In Taiwan, the northeast wind prevails during the autumn and winter seasons, while the southwest wind prevails during the spring and summer seasons. The moderate to strong wind speed ranges

Table 3
Freshwater discharges at upstream boundaries

Upstream boundaries	Freshwater discharge (m^3/s)	
	Q_{50}	Q_{10}
Tahan Stream	11.66	91.7
Hsintien Stream	31.7	149.5
Keelung River	9.35	63.5

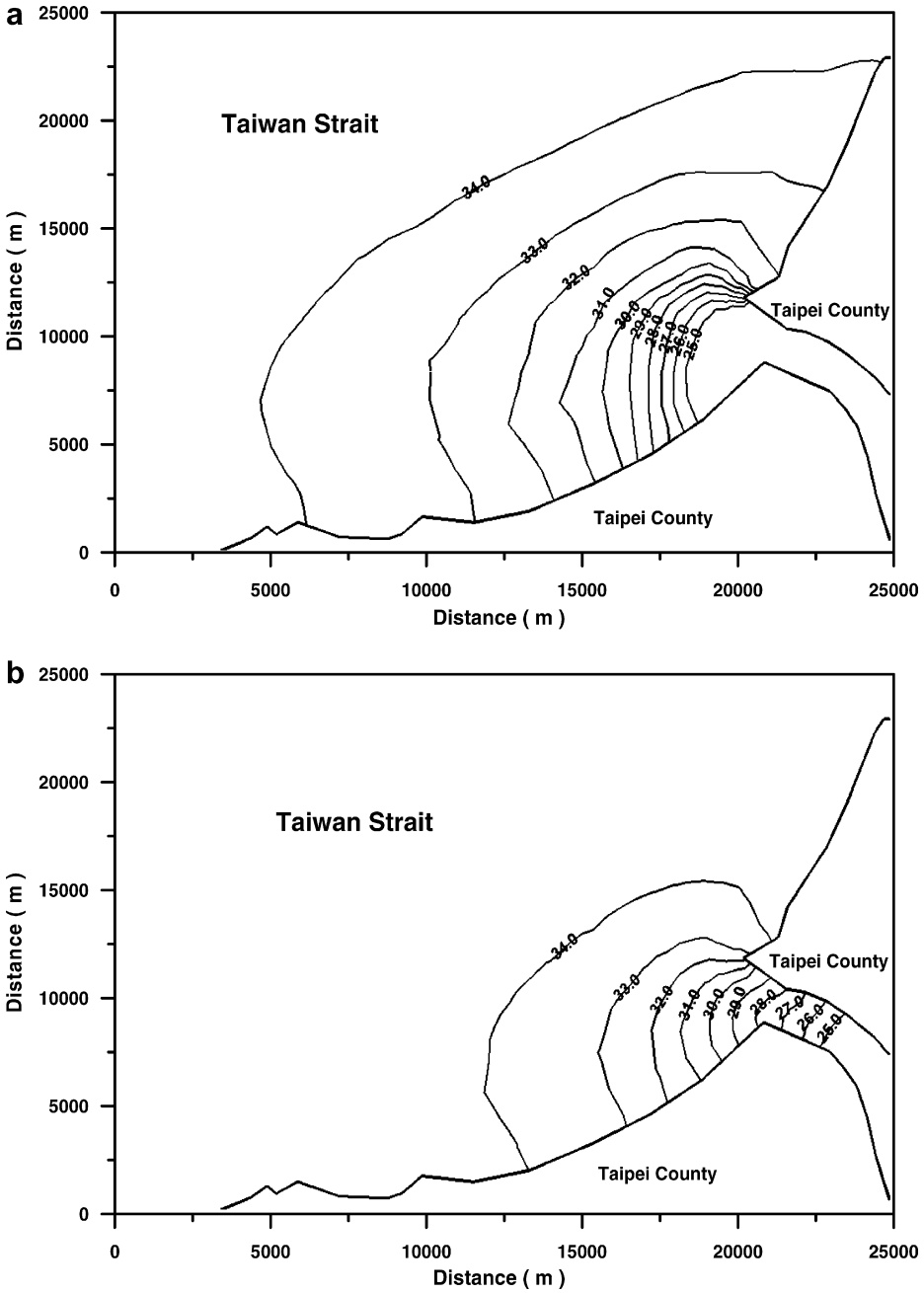

Fig. 7. Surface salinity fields for pure buoyancy forcing under (a) Q_{10} and (b) Q_{50} flow conditions.

from 6 to 15 m/s [23]. Therefore the wind-driven experiments include two main wind directions (coming from northeast and southwest) and employ a magnitude of 10 m/s. The fields of model computed mean surface elevation are shown in Fig. 9. It is interesting to note that significant variation in wind direction cause quite different elevation field and, therefore, circulation pattern. Furthermore, the wind-driven velocity field (Fig. 10) is greatly influenced by the fact that the Danshuei River coastal sea is a topographic steep basin. The present of shallow coastline and deep-sea region enhance the spatial variation of the flow. When the wind direction is from northeast, the mean surface elevation is higher than that wind direction is from southeast

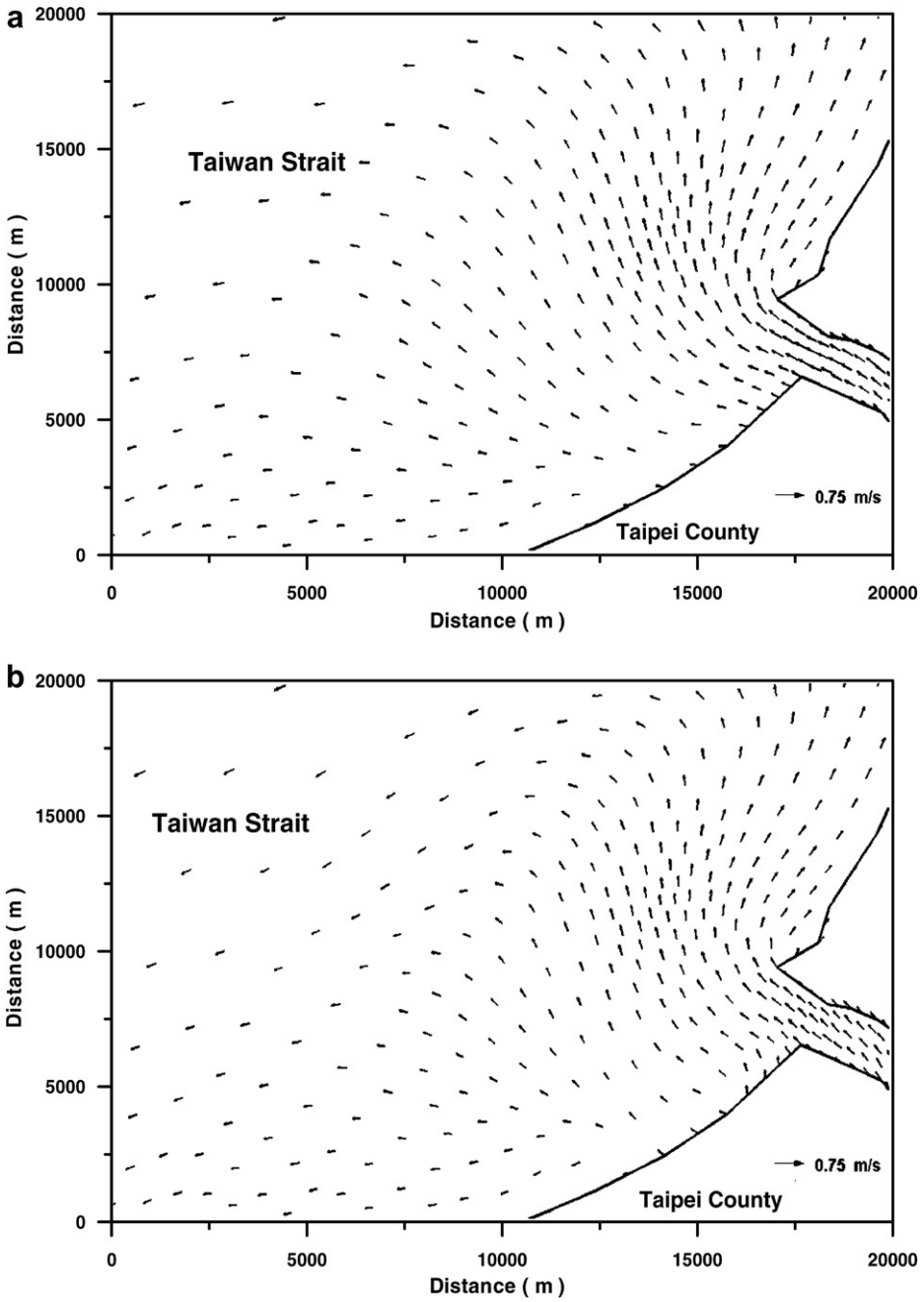

Fig. 8. Surface residual current for pure buoyancy forcing under (a) Q_{10} and (b) Q_{50} flow conditions.

(Fig. 9). When the wind direction is from northeast, the residual current is higher than that wind direction is from southeast (Fig. 10).

Fig. 11 presents the tidally averaged salinity distribution with different wind direction. Because no freshwater discharges are considered in the model simulation, the plume of saline water is confined at the Danshuei River mouth. However, the wind direction also affects the upwelling/downwelling of the saline water. In the case of model simulation, the wind stress and tidal forcing are included. The results reveal that the wind direction has a dominant effect on the velocity field in the Danshuei River coastal sea.

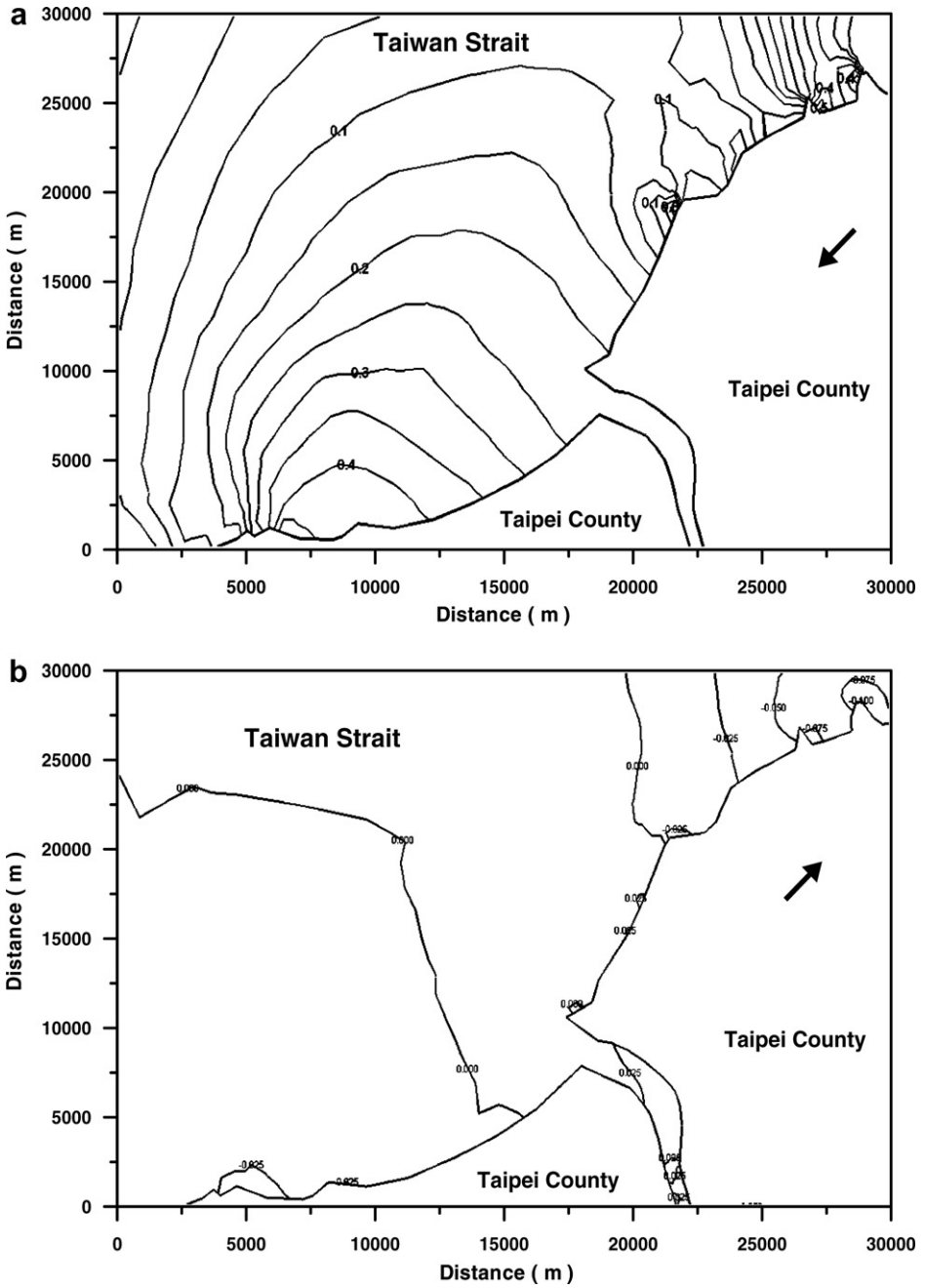

Fig. 9. Mean surface elevation fields (in meter) for pure wind stress forcing (10 m/s); wind direction is from (a) Northeast and (b) Southeast.

5.3. The combined effect of buoyancy and wind stress

The combined effect of wind-driven (barotropic), buoyancy-driven (baroclinic), and tidal forcing is investigated in the model simulation. Two simulations, corresponding to the main wind directions (southwest and northeast) have been performed. The wind intensity is assumed 10 m/s and the Q_{10} freshwater discharge from the upriver boundaries (i.e. Tahan Stream, Hsintien Stream, and Keelung River) is imposed. Five tidal constituents, M_2, S_2, N_2, K_1, and O_1, are also forced at the sea boundaries (see Table 1).

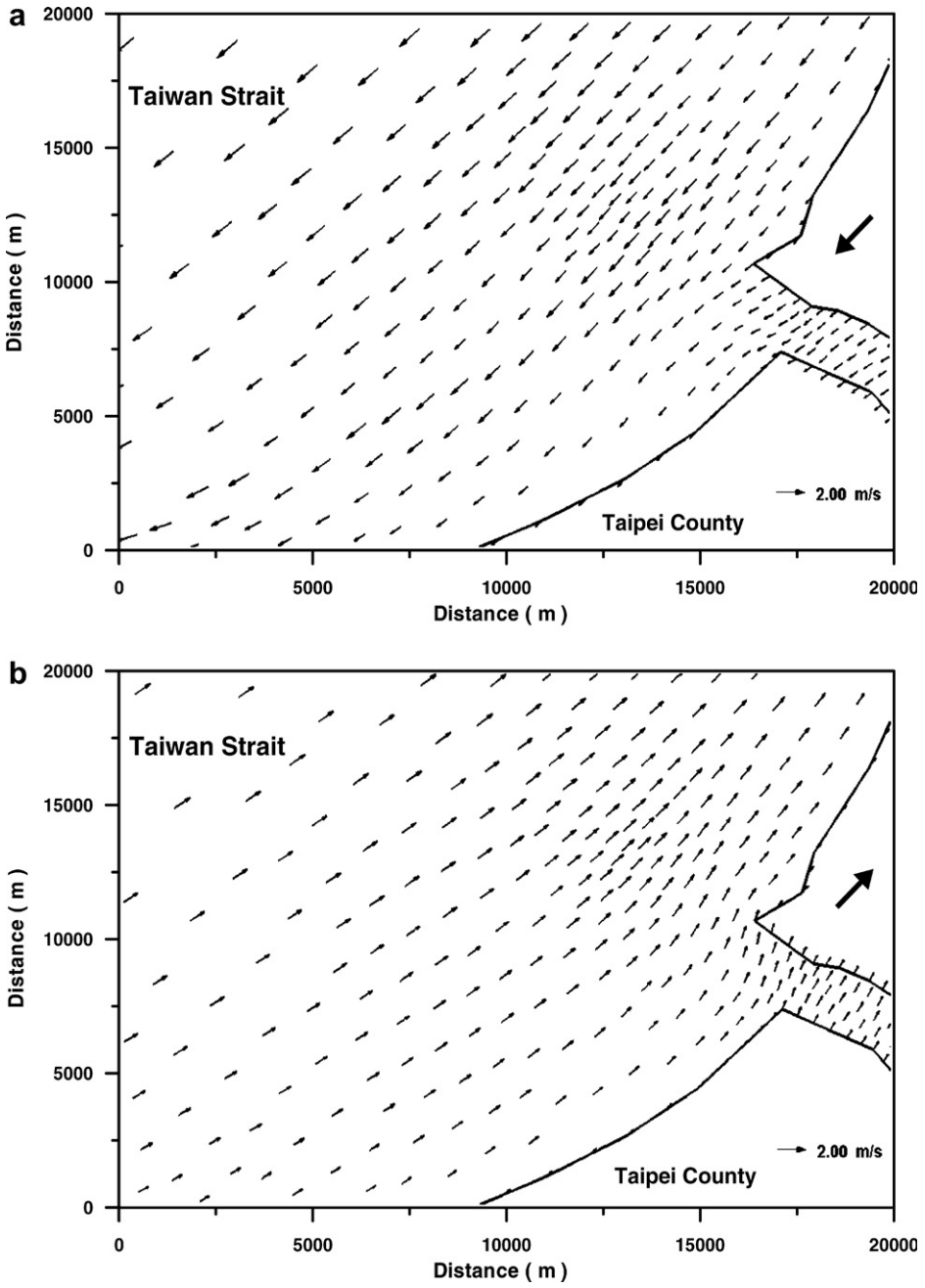

Fig. 10. Surface residual current for pure wind stress forcing (10 m/s); wind direction is from (a) Northeast and (b) Southeast.

Fig. 12 shows the surface plume of tidally averaged salinity distribution under wind directions, southwest and northeast. When winds are downwelling-favorable, the surface low-salinity waters are flushed out and move to southwest coast. Conversely, large amounts of low-salinity water flushed out the Danshuei River mouth during upwelling-favorable winds, as the buoyancy-driven circulation is reversed (Fig. 13). In this study of wind action on estuarine plume, Chao [5] obtained similar circulation and notes that surface currents are dominated by wind-induced Ekman drifts. He also mentioned that when the wind is parallel to the coast and downwelling favorable, it reinforces the coastal jet, pushing the surface light water and enhancing the stratification.

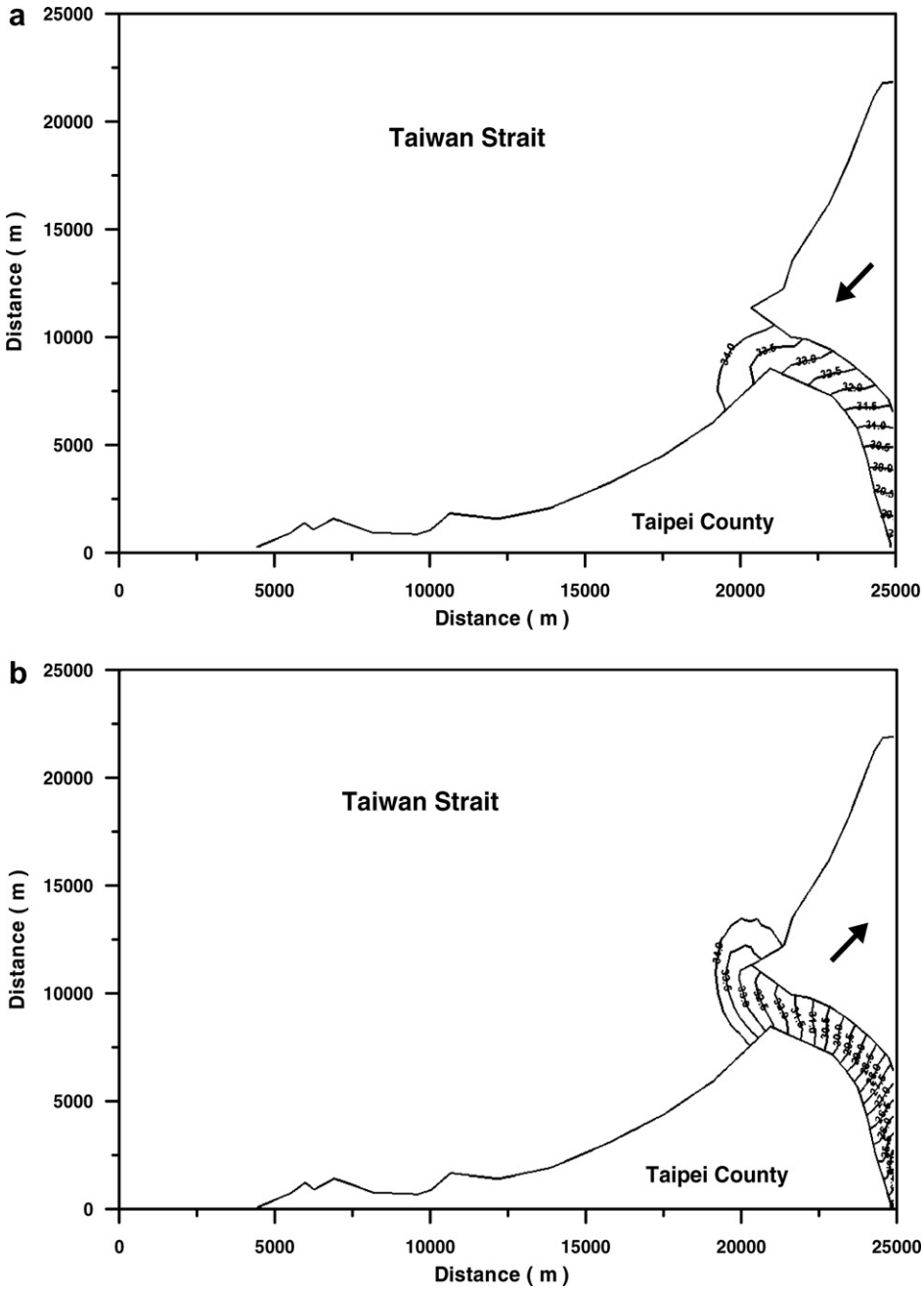

Fig. 11. Surface salinity fields for pure wind stress forcing (10 m/s); wind direction is from (a) Northeast and (b) Southeast.

The velocity fields (Fig. 13) exhibit the strongest southwest and northeast coastal current depended on the wind directions; this current has a wind-driven (barotropic) and buoyancy-driven (baroclinic) component. The flow field is reduced at the shallow coastline. In both cases the circulation is largely modified by wind stresses. As mentions in Chao [5], the surface circulation is affected by Ekman drift. This circulation leads to a new shape for the surface plume. On the other hand, residual bottom water circulations are less affected by wind surface stress (not shown). In the case of model simulation, the freshwater discharge, wind stress, and tidal

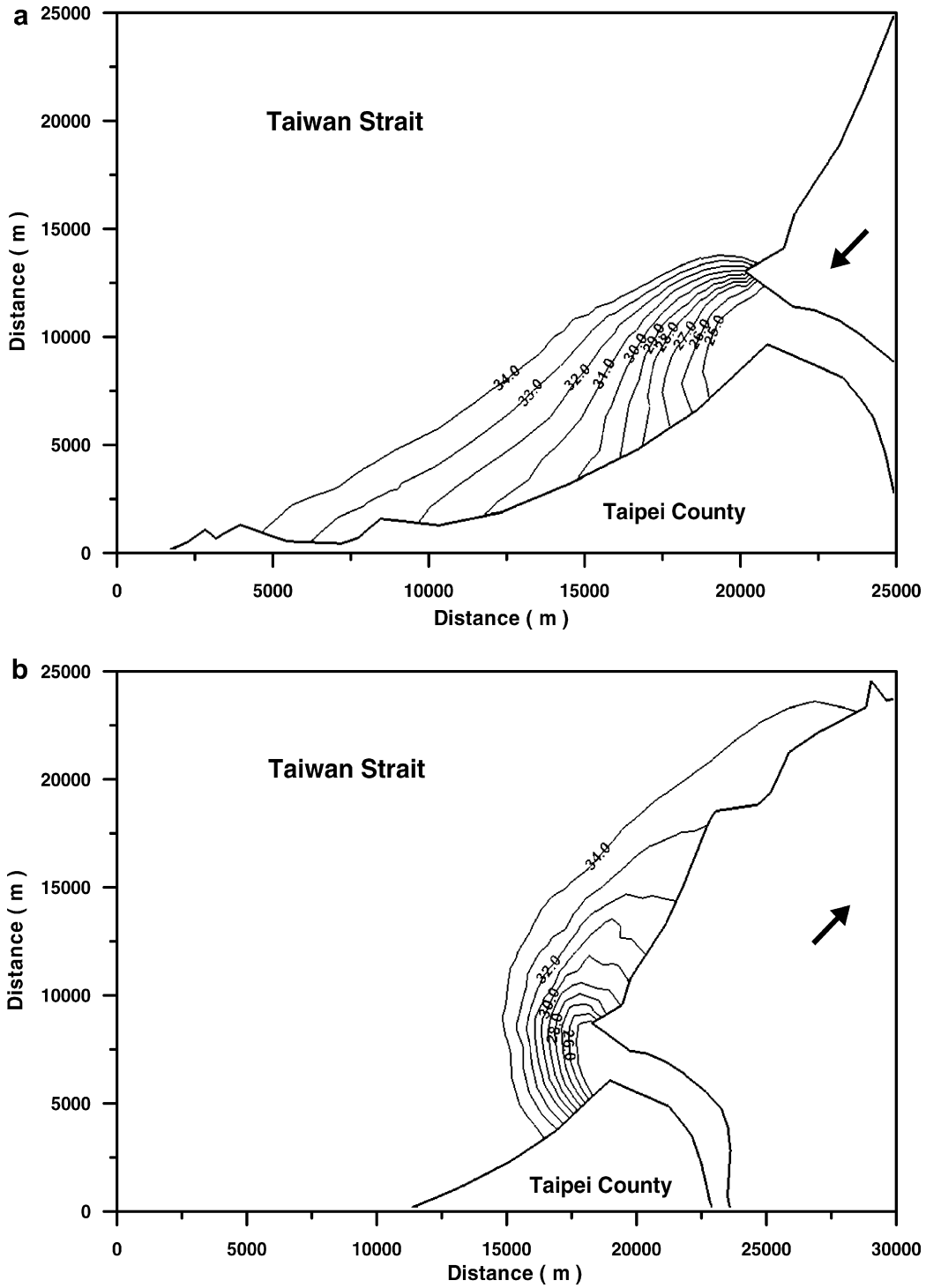

Fig. 12. Surface salinity fields for buoyancy and wind stress forcings; wind direction is from (a) Northeast and (b) Southeast.

forcing are included. The results reveal that the combination of wind-driven and buoyancy-driven enhances the plume region along the Danshuei River coastal area.

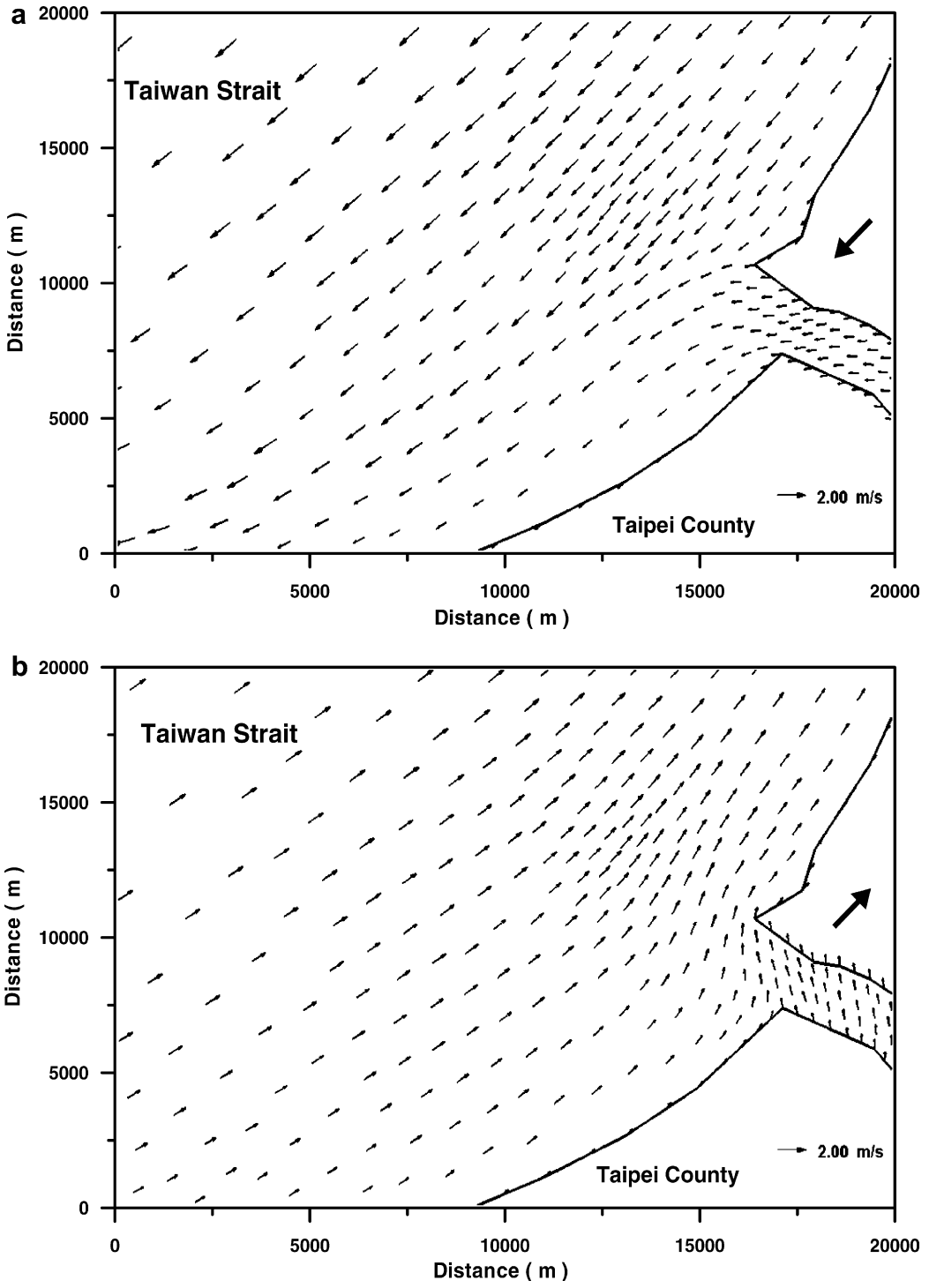

Fig. 13. Surface residual current for buoyancy and wind stress forcings; wind direction is from (a) Northeast and (b) Southeast.

6. Conclusions

A three-dimensional numerical hydrodynamics model, UnTRIM, was implemented and applied to the Danshuei River estuarine system and its adjacent coastal sea in northern Taiwan. The model was calibrated

against five major astronomical tides through the adjustment the bottom friction coefficient represented by Manning–Chezy formula. The final model calibration was accomplished when the tidal amplitudes and phases of these astronomical tidal constituents were accurately reproduced. The model was further verified by comparing directly with field measured water surface elevation, current and salinity under variable daily freshwater discharges from upriver of the Tahan Stream, Hsintien Stream, and Keelung River in year 2000.

The verified model was then applied to investigate the influence of wind stress and freshwater discharge on Danshuei River plume. The numerical experiments were conduced with three cases with buoyancy-driven forcing, wind stress forcing, and combined effect of buoyancy and wind stress. In these three cases, the tidal influences are included in the model simulations. The results reveal that when winds are downwelling-favorable, the surface low-salinity waters are flushed out and move to southwest coast. Conversely, large amounts of low-salinity water flushed out the Danshuei River mouth during upwelling-favorable winds, as the buoyancy-driven circulation is reversed. If the pure freshwater discharge and tidal forcing are included, the magnitude of buoyancy-driven significantly affects the plume distance from the Danshui River mouth to adjacent coastal sea. In the case of model simulation, the freshwater discharge, wind stress, and tidal forcing are included. The results reveal that the combination of wind-driven and buoyancy-driven enhances the plume region along the Danshuei River coastal area.

Acknowledgements

The project, under which this study was conducted, was supported by the National Science Council, Taiwan, under grant number 94-2211-E-239-011. The financial support is highly appreciated. We also thank the Taiwan Water Resources Agency, Industrial Technology Institute, and Central Weather Bureau for providing the prototype data. The authors also would like to express their appreciation to the manuscript reviewers; through their comments this paper was substantially improved.

References

[1] V.H. Kourafalou, L.Y. Oey, J.D. Wang, T.N. Lee, The fate of river discharge on the continental shelf. 1. Modeling the river plume and the inner shelf coastal current, J. Geophys. Res. 101 (C2) (1996) 3415–3434.
[2] V.H. Kourafalou, River plume development in semi-enclosed Mediterranean regions: North Adriatic Sea and Northwestern Aegean Sea, J. Mar. Syst. 30 (3–4) (2001) 181–205.
[3] T.W. Kao, The dynamics of small scale fronts; Part I. Shelf water structure due to freshwater discharge, J. Phys. Oceanogr. 11 (1981) 1215–1223.
[4] R.W. Garvine, Estuary plumes and fronts in shelf waters: a layer model, J. Oceanogr. 17 (1987) 1877–1896.
[5] S.Y. Chao, River-forced estuarine plumes, J. Phys. Oceanogr. 18 (1988) 72–88.
[6] L.Y. Oey, G.L. Mellor, Subtidal variability of estuarine outflow, plume and coastal current: a model study, J. Phys. Oceanogr. 23 (1) (1993) 164–171.
[7] A.E. Yankovsky, D.C. Chapman, A simple theory for the fate of buoyant coastal discharge, J. Phys. Oceanogr. 27 (1997) 1386–1401.
[8] V.H. Kourafalou, T.N. Lee, L.Y. Oey, J.D. Wang, The fate of river discharge on the continental shelf 2. Transport of coastal low-salinity waters under realistic wind and tidal forcing, J. Geophys. Res. 101 (C2) (1996) 3435–3455.
[9] E.N. Mikhailova, N.B. Shapiro, Modelling of propagation and transformation of riverine waters on a northwestern shelf and in an abyssal part of the Black Sea, J. Phys. Oceanogr. 8 (3) (1997) 169–177.
[10] R.W. Garvine, Penetration of buoyant coastal discharge onto the continental shelf: A numerical model experiment, J. Phys. Oceanogr. 29 (1999) 1892–1909.
[11] I.G. Berdeal, B.M. Hickey, M. Kawase, Influence of wind stress and ambient flow on a high discharge river plume, J. Geophys. Res. 107 (C9) (2002) 3130–3153.
[12] S. Arnoux-Chiavassa, V. Rey, P. Fraunie, Modeling 3D Rhone river plume using a higher order advection scheme, Oceanol. Acta 26 (2003) 299–309.
[13] G. Lacroix, K. Ruddick, J. Ozer, C. Lancelot, Modelling the impact of the Scheldt and Rhine/Meuse plumes on the salinity distribution in Belgian water (southern North Sea), J. Sea Res. 52 (2004) 149–163.
[14] M.M. Whitney, R.W. Garvine, Simulating the Delaware Bay buoyant outflow: Comparison with observations, J. Phys. Oceanogr. 36 (1) (2006) 3–21.
[15] A.F. Blumberg, Turbulent mixing processes in lakes, reservoirs and impoundments, in: W.G. Gray (Ed.), Physical-based Modeling of Lakes, Reservoirs, and Impoundments, ASCE, 1986, pp. 79–104.
[16] V. Casulli, R.T. Cheng, Semi-implicit finite difference methods for three-dimensional shallow water flow, Int. J. Numer. Methods Fluids 15 (1992) 629–648.

[17] V. Casulli, R.V. Walters, An unstructured grid, three-dimensional model based on the shallow water equations, Int. J. Numer. Methods Fluids 32 (2000) 331–348.
[18] V. Casulli, P. Zanolli, Semi-implicit modeling of nonhydrostatic free-surface flows for environmental problems, Math. Comput. Modell. 36 (9–10) (2002) 1131–1149.
[19] C. Chen, H. Liu, An unstructured grid, finite-volume, three-dimensional, primitive equations ocean model: application to coastal and estuaries, J. Atmos. Ocean. Technol. 20 (2003) 159–186.
[20] S. Sankaranarayanan, A 3D boundary-fitted barotropic hydrodynamic model for the New York Harbor region, Contin. Shelf Res. 25 (18) (2005) 2233–2260.
[21] L. Zhong, M. Li, Tidal energy fluxes and dissipation in the Chesapeake Bay, Contin. Shelf Res. 26 (6) (2006) 752–770.
[22] R.T. Cheng, V. Casulli, Evaluation of the UnTRIM model for 3-D tidal circulation, Proc. 7th Int. Conf. Estuarine Coast. Model., Florida (2001) 628–642.
[23] S.F. Su, Variation of Tidal Current Vertical Structure at Tanshui Estuary Region of Freshwater Influence. M.Sc. thesis, National Sun Yat-Sen University, 2006 (in Chinese).
[24] M.H. Hsu, A.Y. Kuo, J.T. Kuo, W.C. Liu, Procedure to calibrate and verify numerical models of estuarine hydrodynamics, ASCE J. Hydraul. Eng. 125 (2) (1999) 166–182.
[25] W.C. Liu, M.H. Hsu, A.Y. Kuo, Investigation of long-term transport in Tanshui River estuary, Taiwan, ASCE J. Waterway, Port, Coastal, Ocean Eng. 127 (2) (2001) 61–71.
[26] W.C. Liu, M.H. Hsu, A.Y. Kuo, J.T. Kuo, The influence on river discharge on salinity intrusion in the Tanshui River estuary, Taiwan, J. Coastal Res. 17 (3) (2001) 544–552.
[27] W.C. Liu, M.H. Hsu, C.R. Wu, C.F. Wang, A.Y. Kuo, Modeling salt water intrusion in Tanshui River estuarine system-Case-study contrasting now and then, ASCE J. Hydraul. Eng. 130 (9) (2004) 849–859.
[28] Y.H. Wang, Mapping flow using towed-ADCP in coastal water of Taiwan, Proc. 24th Ocean Eng. Conf. Taiwan (2002) 485–490, in Chinese.
[29] K.F. Bowden, P. Hamilton, Some experiments with a numerical model of circulation and mixing in tidal estuary, Est. Coast. Mar. Sci. 3 (3) (1975) 281–301.
[30] V. Casulli, E. Cattani, Stability accuracy and efficiency of a semi-implicit method for three-dimensional shallow water flow, Comput. Math. Appl. 27 (1994) 99–112.
[31] V. Casulli, G.S. Stelling, Numerical simulation of 3D quasi-hydrostatic free-surface flows, ASCE J. Hydraul. Eng. 124 (7) (1998) 678–686.
[32] S. Rebay, Efficient unstructured mesh generation by means of Delaunay triangulation and Bowyer-Watson algorithm, J. Comput. Phys. 106 (1993) 125–138.
[33] R.T. Cheng, J.R. Burau, J.W. Gartner, Interfacing data analysis and numerical modelling for tidal hydrodynamic phenomena, in: B.B. Parker (Ed.), Tidal Hydrodynamics, John Wiley & Sons, New York, 1991, pp. 201–219.
[34] R.T. Cheng, J.W. Garnter, V. Casulli, Tidal, residual, intertidal mudflat (TRIM) model and its applications to San Francisco Bay, California, Est., Coast., Shelf Sci. 36 (3) (1993) 235–280.
[35] R. Bradbury, User's guide for Argus One, Argus Interware, Inc, 1997.
[36] S. Jan, Y.H. Wang, S.Y. Chao, D.P. Wang, Development of a nowcast system for the Taiwan Strait (TSNOW): numerical simulation of barotropic tides, Ocean Polar Res. 23 (3) (2001) 195–203.